SMALL SCALE HEATER TESTS IN ARGILLITE OF THE ELEANA FORMATION AT THE NEVADA TEST SITE

D. F. MCVEY, R. K. THOMAS, AND A. R. LAPPIN

SAND79-0374
Unlimited Release

SMALL SCALE HEATER TESTS IN ARGILLITE OF THE ELEANA FORMATION AT THE NEVADA TEST SITE

D. F. McVey, R. K. Thomas, and A. R. Lappin
Sandia Laboratories
Albuquerque, NM 87185

November 1979

ABSTRACT

A series of near-surface heater tests has been run in the Eleana Formation at the Department of Energy's Nevada Test Site, in an effort to evaluate argillaceous rock as a potential emplacement medium for nuclear waste storage. The main test, which employed a full-scale heater with a thermal output approximating that which would be expected from commercial borosilicate waste, was designed to operate for several months. Two smaller, scaled tests were run prior to the full-scale test, in order to determine the basic feasibility of operating the full-scale test as planned. This report develops the thermal scaling laws, describes the pretest thermal and thermomechanical analysis conducted for these two tests, and discusses the material properties data used in the analyses. The predictions are compared with qualitative experimental results. In the first test, scaled to a large heater of 3.5 kW power, computed heater temperatures were within 7% of measured values for the entire 96 hour test run. The second test, scaled to a large heater having 5.0 kW power, experienced periodic water in-flow onto the heater, which tended to damp the temperature. For the second test, the computed temperatures were within 7% of measured for the first 20 hours. After this time, the water effect became significant and the measured temperatures were 15-20% below those predicted. On the second test, rock surface spallation was noted in the bore hole above the heater, as predicted. The scaled tests indicated that in situ argillite would not undergo major thermostructural failure during the follow-on, 3.5 kW, full-scale test.

CONTENTS

FIGURES

FIGURES (cont)

TABLES

NOMENCLATURE

A	Area, m^2
E	Elastic modulus, MPa
F_{i-o}	Combined geometrical shape and emissivity factor
$J_2^{\frac{1}{2}}$	Deviatoric stress invariant, MPa
K	Rock thermal conductivity, J/m-hr-^oC
L_o	Heater length, m
P	Power, J/hr
p	Bulk pressure, MPa
Q'''	Volumetric heating rate, J/m^3-hr
Q	Heat generation rate, J/hr
r	Radial dimension, m
R	Radial dimension, m
$\overline{T}$	Non-dimensional temperature
t	Temperature, ^oC or K
V	Volume, m^3
Z	Axial dimension, m
α	Thermal diffusivity, m^2/hr
α_T	Linear thermal expansion coefficient, $^oC^{-1}$
ε	Emittance
ν	Poisson's ratio
θ	Time, hr
σ	Stefan-Boltzmann constant, J/m^2-hr-K^4
$\sigma_1, \sigma_2, \sigma_3$	Principal stresses, MPa

NOMENCLATURE (cont)

Superscripts

—	Non-dimensional

Subscripts

i	Heater radius
m	Model or scaled
o	Hole radius, reference dimension
p	Prototype or full scale prototype
r	Rock

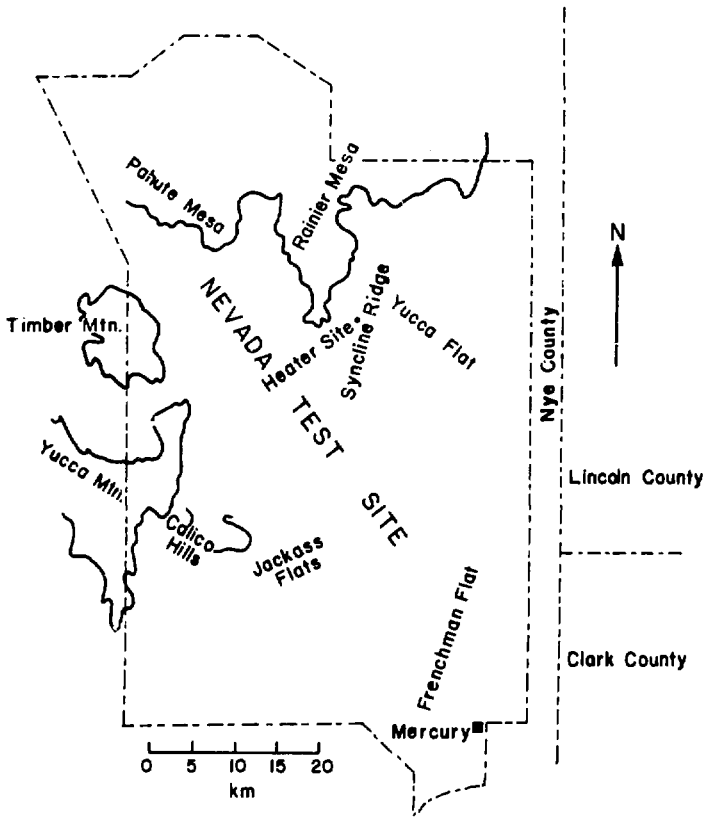

FIGURE 1. Map of Nevada Test Site, Showing Experiment Locality.

INTRODUCTION

The United States Department of Energy, Nevada Operations Office, is sponsoring a project at the Nevada Test Site to investigate the suitability of several "hard rock" media for use as a high level waste repository. One of the media being considered is argillite, a slightly metamorphosed shale which occurs within the Eleana formation. Specific argillite occurrences are located near Syncline Ridge in the north central region of the test site and in Topopah Wash (Calico Hills) in the southwestern portion of the test site (see Figure 1).

The investigations at Syncline Ridge include operation of a full-scale, near-surface heater test in which an electrically powered heater, 0.32 m diameter x 3.0 m heated length, was inserted into a 21.3 m deep x 0.36 m diameter hole drilled in the argillite. The heater dimensions roughly approximate those of waste canisters currently being considered. A constant power output of 3.5 kW was selected for this test in order to approximate the initial heat production from a canister of this size filled with ten-year-old waste encapsulated in borosilicate glass. This waste form was assumed, rather than UO_2 spent fuel of the same age, since the early time heat production of conventional borosilicate high level waste (HLW) represents a greater thermal load. The thermal load, therefore, was assumed to approximate the upper limit of the most likely commercial wastes. A test time on the order of one year is desired to obtain temperatures near the maximum anticipated service temperature.

Prior to running the large heater experiment, two small heater tests were run to obtain qualitative data on the thermomechanical response of near-surface, in situ argillite. The heater used in these tests had a 0.089 m diameter with a 1.22 m heated length. For the small test design, thermal scaling laws were derived to define test duration and heater power levels such that the thermal response of the argillite would scale, or model, the response to the large or

full-scale heater. Two power levels were used in the scaled tests: 1.4 kW, scaled to a full-scale heater power of 3.5 kW, and 2.0 kW, scaled to about 1.4 times that of the full-scale heater.

The scale tests were designed to obtain only qualitative data. Power input and heater surface temperature as functions of time were recorded. Argillite thermomechanical response was inferred by comparison of pre and posttest bore hole scans taken with a bore hole TV camera and recorded on video tape.

This report documents the pre and posttest analyses and the operation of the scale experiments. It also discusses the data obtained from the scale tests. The predicted thermal response of the large and small heaters are time scaled and compared. Measured heater temperature histories are compared to predictions. Computed thermal stress levels are compared with laboratory derived failure criteria, and observed surface spallation of the argillite hole is described by means of bore hole pictures.

TEST THERMAL SCALING

In the original concept of the small heater test, the heater and bore hole dimensions and the heater power levels were to be scaled such that full geometric similarity would be obtained between the model (small) and the prototype (full-scale) test results. To this end, scaling laws were derived by nondimensionalizing the appropriate conduction heat transfer equation and boundary conditions. The conduction equation in cylindrical coordinates, assuming constant, isotropic thermal properties is

$$\frac{\partial^2 t}{\partial r^2} + \frac{1}{r}\frac{\partial t}{\partial r} + \frac{\partial^2 t}{\partial z^2} = \frac{1}{\alpha}\frac{\partial t}{\partial \theta} \quad . \tag{1}$$

Assuming one-dimensional heat transfer between the heater and rock surface, the boundary condition at the outside of the hole is

$$q = -KA\frac{\partial t}{\partial r} \text{ @ } r = R_o \quad .$$

Non-dimensionalizing Equation (1) with

$$\bar{T} = \frac{t}{T_o} \qquad \bar{R} = r/R_o \qquad \bar{Z} = Z/L_o \qquad \bar{\theta} = \frac{\theta\alpha}{R_o^2} \quad , \tag{2}$$

yields

$$\frac{T_o}{R_o^2}\frac{\partial^2\bar{T}}{\partial\bar{R}^2} + \frac{T_o}{R_o^2}\frac{1}{\bar{R}}\frac{\partial\bar{T}}{\partial\bar{R}} + \frac{T_o}{L_o^2}\frac{\partial^2\bar{T}}{\partial\bar{Z}^2} = \frac{T_o}{\frac{\alpha R_o^2}{\alpha}}\frac{\partial\bar{T}}{\partial\bar{\theta}} \quad ,$$

$$\frac{\partial^2\bar{T}}{\partial\bar{R}^2} + \frac{1}{\bar{R}}\frac{\partial\bar{T}}{\partial\bar{R}} + \left(\frac{R_o}{L_o}\right)^2\frac{\partial^2\bar{T}}{\partial\bar{Z}^2} = \frac{\partial\bar{T}}{\partial\bar{\theta}} \quad ,$$

and

$$\bar{T} = f\left(\bar{R},\ \bar{Z},\ \frac{R_o}{L_o},\ \frac{\theta\alpha}{R_o^2}\right) \quad . \tag{3}$$

For the model and full scale tests, the non-dimensional temperatures, $\bar{T}$, will be the same at equivalent $\bar{R}$, $\bar{Z}$ for the same value of non-dimensional time $\bar{\theta} = \theta\alpha/R_o^2$ if the non-dimensional heated length, L_o/R_o, is the same in the two tests and the boundary conditions are properly scaled.

The boundary condition was scaled for the case of a constant volumetric power generation input to the rock surface. Assuming losses and axial transfer of heat in the heater to be zero,

$$\text{total heat generated} = \text{heat into surface} \quad ,$$

$$P = Q'''(\pi R_i^2 L_o) = -2\pi R_o L_o K\frac{\partial t}{\partial r} \quad .$$

Non-dimensionalizing with parameters from Equation (2) results in

$$\frac{Q'''}{2}\frac{\bar{R}_i^2 R_o^2}{\bar{R}_o R_o} = \frac{-KT_o}{R_o}\frac{\partial\bar{T}}{\partial\bar{R}} \quad ,$$

$$\bar{R}_o = 1 \quad ,$$

$$\frac{Q'''R_o^2}{2KT_o}\bar{R}_i^2 = -\frac{\partial \bar{T}}{\partial \bar{R}} \quad . \tag{4}$$

For a model/prototype, i.e., scaled/full scale, system having complete geometric similarity, constructed of the same material and at the same reference temperature, the following equations hold:

$$\bar{L}_{o_m} = \bar{L}_{o_p} \; ; \; \bar{R}_{i_m} = \bar{R}_{i_p} \; ; \; \alpha_m = \alpha_p \; ; \; T_{o_m} = T_{o_p} \quad .$$

Using dimensions for the scaled and full scale heaters,

$$R_{o_m} = 2 \text{ inches} \qquad R_{o_p} = 7 \text{ inches} \quad ,$$

the similarity parameters and scale factors for the heater tests are computed and shown in Table I.

TABLE I

SIMILARITY PARAMETERS AND SCALE FACTORS FOR GEOMETRICALLY SCALED HEATER TEST

Characteristic	Similarity Parameter	Scale Factor
Geometric Scale	Bore Hole Radius	$R_{o_m}/R_{o_p} = 2/7$
Time Scale	Fourier Number $\left(\frac{\theta\alpha}{R_o^2}\right)$	$\theta_m = \theta_p/12.25$
Volumetric Heating Rate	$\frac{Q'''R_o^2\bar{R}_i^2}{2KT_o}$	$Q_m''' = 12.25\, Q_p'''$
Total Power Input	$\frac{P}{2\pi R_o \frac{L_o}{R_o} T_o K}$	$P_m = 2/7\, P_p$

From the entry in the time scale row of Table I, it appears that a scale test of about one month is thermally equivalent to a prototype test of one year. In addition, it is noted that to simulate a prototype heater power output of 3.5 kW, a model power output of 1 kW is required if geometric scaling is maintained.

The heating elements to be used for the small heater tests had previously been procured, however with preformed length and radius of curvature. The heating element geometry prevented complete geometric scaling of the experiments. The dimensions of the full scale heater, and the theoretical geometrically scaled heater are given in Table II, as well as the model heater constructed from the preformed heating elements.

TABLE II

COMPARISON OF HEATER DIMENSIONS

	R_o Hole Radius (in)	R_i Heater Radius (in)	L_o Heated Length (ft)	$L_o/2R_i$ Heater L/D	R_o/R_i
Full Scale Heater	7.0	6.375	10	9.41	1.098
Scaled* Heater	2.0	1.821	2.857	9.41	1.098
Model** Heater	2.0	1.750	4.0	13.71	1.143

*Dimensions based on 2/7 scale factor.

**Dimensions of the heater actually fielded.

As can be seen in Table II, the major scaling discrepancy was in heater length. The model heater fielded had an L/D about 1.46 times that of the true-scale heater (see Table II). As a result of the changes in dimensions, some alterations in the power scaling were required.

Considering the heat flux boundary condition from Equation (4),

$$\left(\frac{Q'''R_o^2}{2KT_o}\bar{R}_i^2\right)_m = \left(\frac{Q'''R_o^2}{2KT_o}\bar{R}_i^2\right)_p ,$$

since the material and reference temperatures are the same,

$$\left(Q'''R_o^2\bar{R}_i^2\right)_m = \left(Q'''R_o^2R_i^2\right)_p ,$$

and,

$$Q'''_m = \left(\frac{R_{o_p}}{R_{o_m}}\right)^2\left(\frac{\bar{R}_{i_p}}{\bar{R}_{i_m}}\right)^2 Q'''_p .$$

Substituting values from Table II,

$$Q_m''' = \left(\frac{7}{2}\right)^2 \left(\frac{6.375/7}{1.75/2}\right)^2 Q_p''' \quad ,$$

$$Q_m''' = (12.25)(1.0833) Q_p''' \quad ,$$

$$Q_m''' = 13.27\ Q_p''' \quad . \tag{5}$$

Thus, the heater radius change from correct geometric scale requires an 8.33% increase in volumetric generation rate over a perfectly scaled case.

Next, to determine total power increase required because of the change in length,

$$V_m = \left(\frac{R_m}{R_p}\right)^2 \left(\frac{L_m}{L_p}\right) V_p \quad ,$$

$$V_m = \left(\frac{1.75}{6.375}\right)^2 \left(\frac{4}{10}\right) V_p \quad ,$$

$$V_m = 0.0301\ V_p \quad .$$

From boundary condition considerations, Equation (5),

$$Q_m''' = 13.27\ Q_p''' \quad ,$$

$$P_m = Q_m''' V_m \quad ,$$

$$P_m = 13.27\ Q_p''' \times 0.03\ V_p \quad ,$$

$$P_m = 0.40\ P_p \quad .$$

These considerations result in the input power specifications

$$P_p = 3.5 \text{ kW} \ , \ P_m = 1.4 \text{ kW} \quad ,$$

$$P_p = 5 \text{ kW} \ , \ P_m = 2 \text{ kW} \quad . \tag{6}$$

The increase in heater L/D causes the temperatures near the heater centerline (L/2 station) to increase above those for a properly scaled L/D. This effect can be assessed by reference to Figure 2, which gives the ratio of the calculated steady state* temperature for an L/D of 10 to the steady state temperature for a range of L/D values. Increasing the L/D from 9.4 to 13.7 results in a 12% increase in canister surface temperature at the heater center plane, or L/2 station. Rather than attempt to modify the power input to account for this factor, which tends to be non-uniform along the heater length, it was decided to proceed with the power levels defined in Equation (6).

THERMAL PREDICTIONS

Based on the scaling considerations discussed in the preceding section, a series of computer predictions of the temperature profiles about the prototype and model heaters were made using the finite element thermal code, COYOTE.[1]

A two-dimensional axisymmetric thermal model of the heater and surrounding argillite was constructed. The analysis region consisted of an argillite section 12.62 m long, extending from an inner radius of 0.0508 m to an outer radius of 3.86 m. A 1.22 m long heated region of 0.0445 m radius was longitudinally centered in the hole extending through the argillite. The dimensions of the argillite were sufficiently large that the outer radius and ends could be considered adiabatic for the time period of interest. The argillite and heater regions were divided into 360 quadrilateral, eight node finite elements, with node points at the corners and side midpoints of each element. A computer plot of the element grid near the heater is shown in Figure 3.

Computer runs were made for the model experiment with power inputs of 1.4 and 2.0 kW, which corresponded to prototype (full-scale) experiments with power inputs of 3.5 kW and 5.0 kW, see Equation (6). The 3.5 kW input was chosen as typical of a high level waste, encapsulated in borosilicate glass, while the 5.0 kW input was chosen as an overtest.

* Steady state refers to the point at which the slope of the temperature versus time curve becomes a constant.

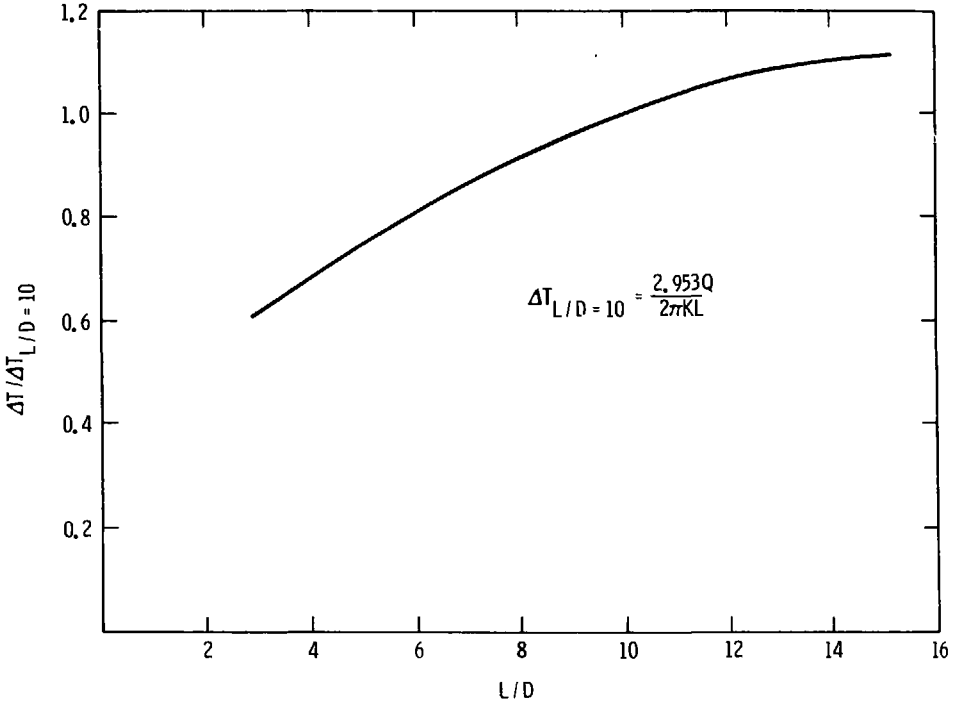

FIGURE 2. Effects of Heater L/D on Maximum Temperature Rise, Relative to Rise for 40 of 10.

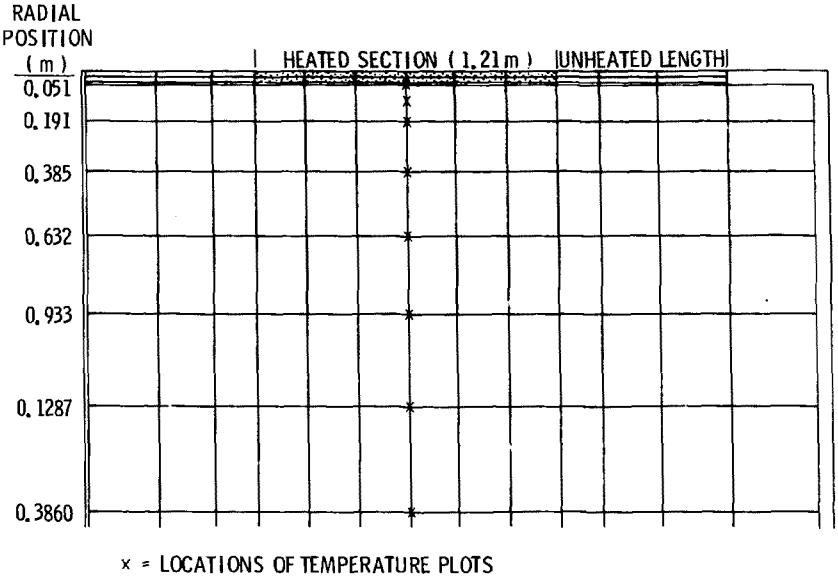

FIGURE 3. Two-Dimensional Axisymmetric Finite Element Thermal Model in the Region Near the Heater.

Argillite thermal properties are shown in Tables III and IV. These data were taken from Reference 2. The conductivity values in columns "F" and "G" of Table III, for radial (normal to the heater axis) and axial (parallel to the heater axis) directions respectively, were used in the analysis, and represent a linear approximation to the experimental data. Conductivities at intermediate temperatures were obtained by linear interpolation. In using the specific heat data, the measured effect of pore water vaporization was removed. Since the samples had partially dried during sample preparation and the exact amounts of water remaining was unknown, the equivalent energy absorption of 3% by weight water was added to the dry rock specific heat. The vaporization was assumed to occur over a temperature range of 55° to 105°C. The thermal properties are discussed in more detail in Appendix A.

Mean argillite density was taken as 2.63 gm/cc. Total normal surface emittance of argillite was assumed to be 0.9.* Emittance of the SS304 stainless steel surface of the heater was taken from data[3] for SS321 oxidized in air at red heat for 30 minutes. The heater emissivities used are tabulated in Table V.

Heat transfer from the heater to the rock was assumed to be one-dimensional combined radiation and conduction through air. Convection was ignored because of indications that the "effective conductivity"** is 1.0 for the range of gap Rayleigh*** numbers encountered in the experimental configuration.[4] Under these assumptions, an effective conductivity across the air gap between the heater and rock may be computed from Equation (7).

---

*Results of similar studies indicate a marked sensitivity of heater and rock skin temperature to heater emissivity, but very limited sensitivity of rock temperature to rock emissivity.

**Ratio of the total heat transferred across a gap by convection and conduction to that transferred by conduction alone.

***The Rayleigh number is a non-dimensional parameter grouping that represents the ratio of the driving force for convection heat transfer to the driving force for conduction heat transfer.

TABLE III

THERMAL CONDUCTIVITY OF ELEANA ARGILLITE
AT ELEVATED TEMPERATURES
(W/m°C)

T(°C)	A	B	C	D	E	F	G
25	-	-	2.43	0.23	2.20-2.71	-	-
50	-	-	2.17	0.06	2.10-2.24	2.3	1.90
75	1.79(1.15)*	1.68	-	-	-	-	-
100†	1.78→1.69	1.67→1.54	2.06	0.11	1.91-2.17	2.2	1.70
150	1.53	1.44	1.80	0.13	1.63-1.91	1.73	1.53
200	1.45	1.39	1.67	0.05	1.62-1.73	1.73	-
250	1.39	1.32	1.69	0.04	1.63-1.72	1.73	-
300	1.36	1.28	1.73	0.09	1.64-1.81	1.73	-
350	1.33	1.24	1.61	0.14	1.55-1.79	1.73	1.33
400	1.31	1.20	1.46	0.11	1.35-1.61	1.60	-
450	1.29	1.17	1.48	0.08	1.33-1.48	1.50	1.29
500	-	-	1.27	0.13	1.12-1.42	1.40	-

A. Axial thermal conductivity, sample UE17e364.

B. Axial thermal conductivity, sample UE17e372.

C. Average of radial conductivities of samples UE17g80, UE17e623, UE17e627, and UE17g68.

D. Standard deviation of measurements in Column C.

E. Range of measurements in Column C.

F. Radial values used in analysis.

G. Axial values used in analysis.

*Value in parentheses measured after measurements at elevated temperatures.

†Decrease in conductivity, indicated by arrow, resulted from holding samples near 100°C for 24 hours.

TABLE IV

RANGES IN SPECIFIC HEAT OF ELEANA ARGILLITE TO 500°C
(BASED ON THREE SAMPLES)

T (°C)	Cp (cal/gm°C)	Used in Analysis** Cp (cal/gm°C)
75	0.23-0.33	0.28
100	0.25-0.40*	0.27
150	0.20-0.24	0.25
400	0.17-0.23	0.20
420	(-)0.56-(+)0.25***	0.20
475	0.18-0.25	0.20
510	0.23-0.39	0.20

*Includes effect of vaporization of an unknown amount of pore water. Smoothed out for this analysis.

**0.290 cal/gm°C added to Cp between 55° and 105°C to account for vaporization of water.

***Includes effect of sulfide reaction.

TABLE V

SURFACE NORMAL EMISSIVITY
FOR STAINLESS STEEL 321

T (K)	ε
300	0.205
400	0.225
500	0.250
600	0.275
700	0.305
800	0.340
900	0.370

Total Heat Transferred = Heat Radiated + Heat Conducted ,

$$\frac{2\pi K_{eff} L_o}{\ln r_o/r_i}(T_i - T_o) = 2\pi L_o r_i F_{i-o}\sigma(T_i^4 - T_o^4) + \frac{2\pi K_{air} L_o}{\ln r_o/r_i}(T_i - T_o) \quad ,$$

$$K_{eff} = \ln\left(\frac{r_o}{r_i}\right) r_i F_{i-o}\sigma\left(\frac{T_i^4 - T_o^4}{T_i - T_o}\right) + K_{air} \quad , \tag{7}$$

where,

$$F_{i-o} = \frac{1}{\frac{1}{\varepsilon_i} + \frac{r_i(1 - \varepsilon_o)}{r_o \varepsilon_o}} \quad .$$

The heater emissivity (ε_i) and air thermal conductivity were input as functions of temperature for the computations. Due to the non-linearity of Equation (7), the surface temperatures of the heater do not scale directly with the Fourier number.* The scale heater will operate at a higher surface temperature than the prototype heater for the same scaled volume power generation. Thus, the scale, model and prototype heater surface temperatures cannot be compared directly.

THERMAL MODELING RESULTS

Computed temperature histories for the model test with 1.4 kW input power are shown in Figures 4 and 5.** Figure 4 gives heater surface temperatures and Figure 5 gives argillite temperatures at eight points radially outward from the L/2 station of the heater (see Figure 3). Calculated isotherm patterns for 1.0, 2.0, 4.0, and 5.0 days are shown in Figure 6. Similar data for the 2.0 kW test

*Non-dimensional time; $F_o = \theta\alpha/R_o^2$.

**Temperature curves and isotherms in this report are presented as plotted by the computer, and have not been smoothed to remove irregularities resulting from the fact that the finite elements used are not infinitely small.

are shown in Figures 7, 8, and 9. The predicted rock surface temperature for the 2 kW test is 120°C higher at the end of 5 days than the surface temperature for the 1.4 kW test. The 50°C isotherm penetrated about 0.61 m from the heater surface in 5 days with 2.0 kW input, while the 50°C isotherm penetrated 0.49 m in 5 days with 1.4 kW input.

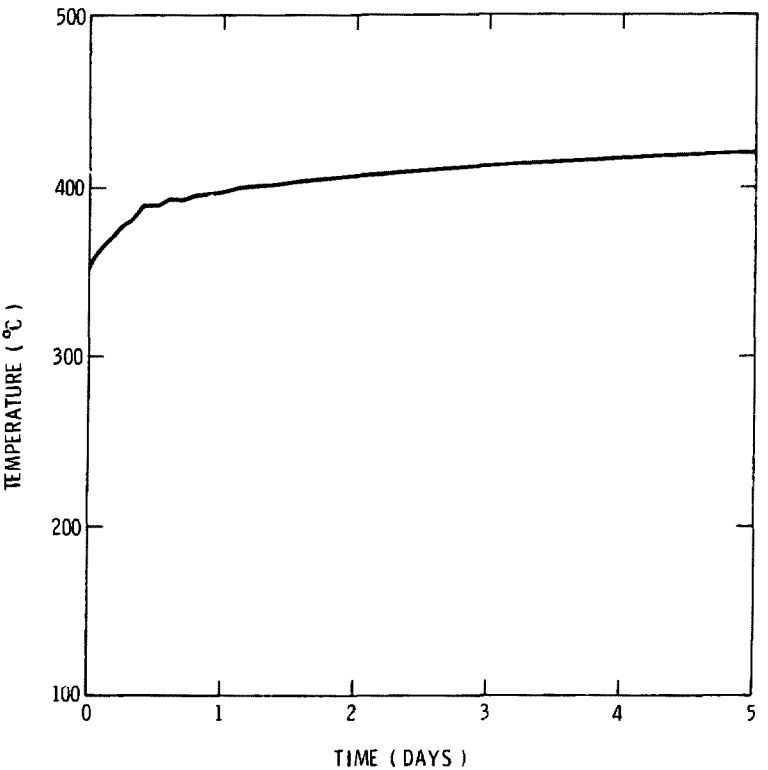

FIGURE 4. CALCULATED MODEL HEATER SURFACE TEMPERATURE AS A FUNCTION OF TIME; 1.4 kW INPUT POWER.

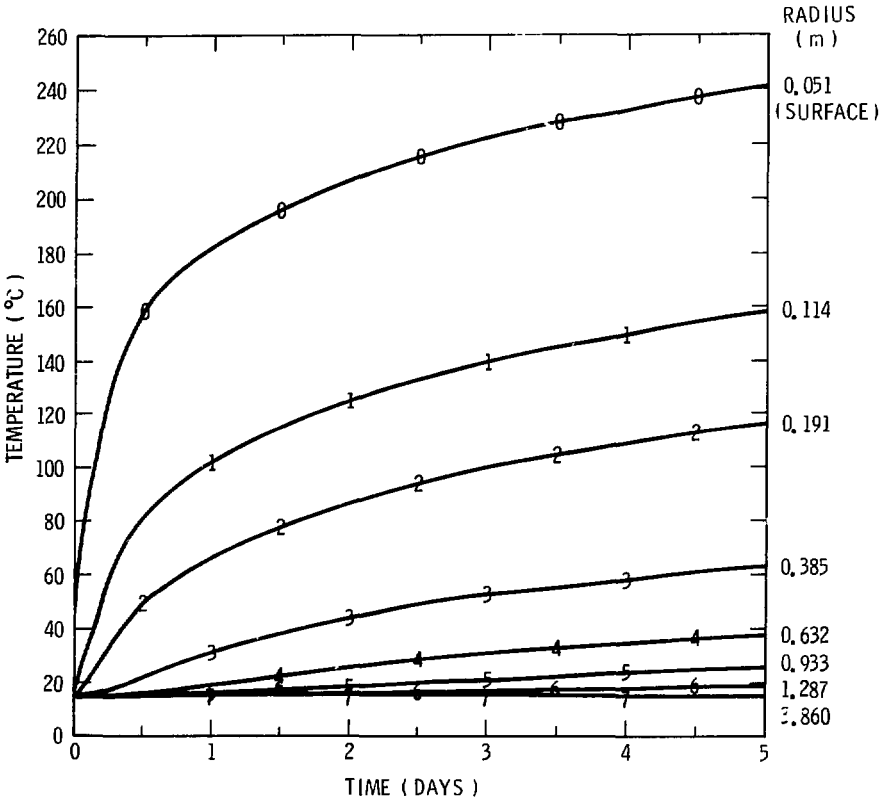

FIGURE 5. CALCULATED TEMPERATURE HISTORIES RADIALLY OUTWARD FROM STATION L/2 OF THE HEATED SECTION OF THE MODEL HEATER; 1.4 kW INPUT POWER.

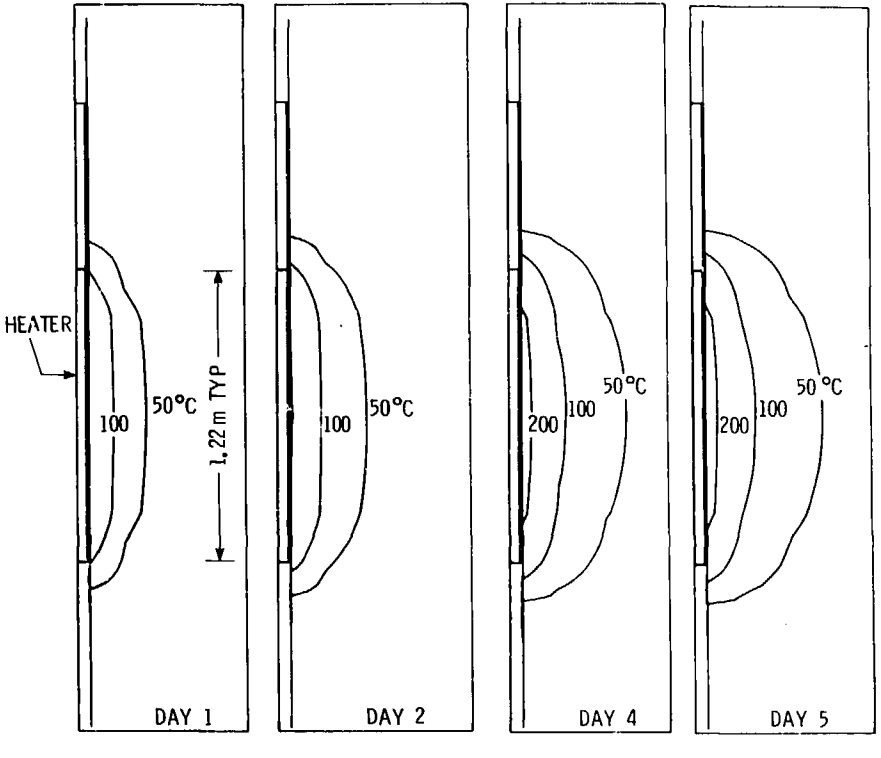

FIGURE 6. ISOTHERMS AT FOUR TIMES FOR MODEL HEATER; 1.4 kW INPUT POWER.

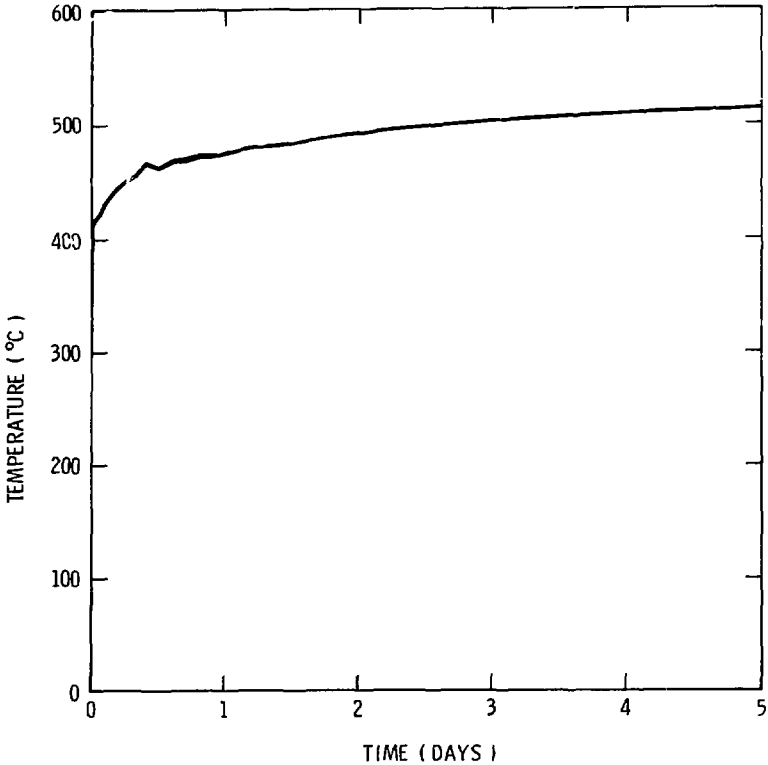

FIGURE 7. CALCULATED MODEL HEATER SURFACE TEMPERATURE AS A FUNCTION OF TIME; 2.0 kW INPUT POWER.

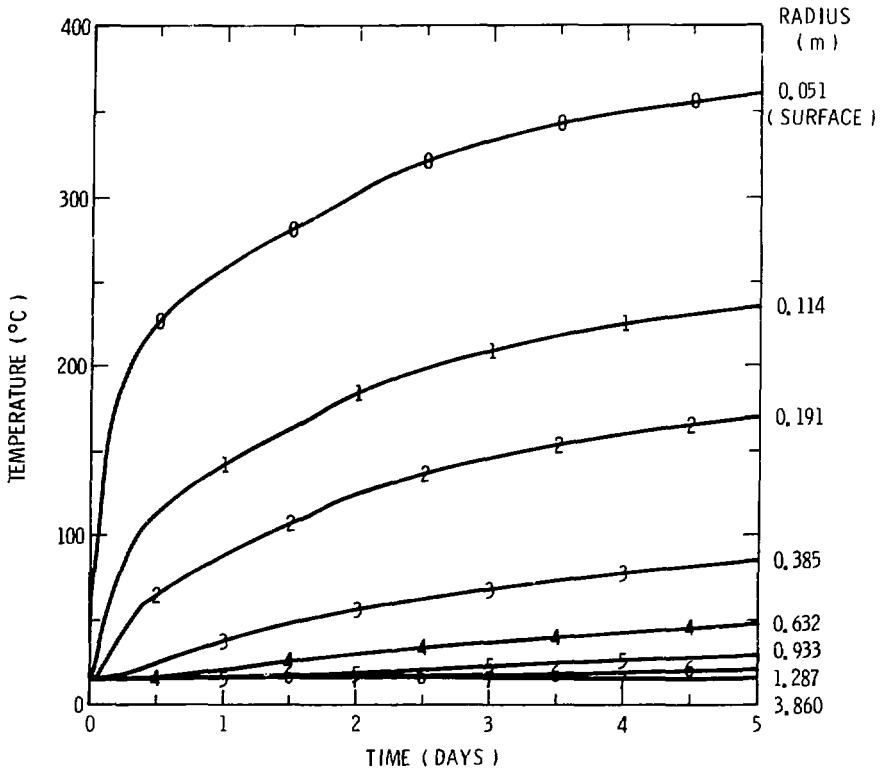

FIGURE 8. CALCULATED TEMPERATURE HISTORIES RADIALLY OUTWARD FROM STATION L/2 OF THE HEATED SECTION OF THE MODEL HEATER; 2.0 kW INPUT POWER.

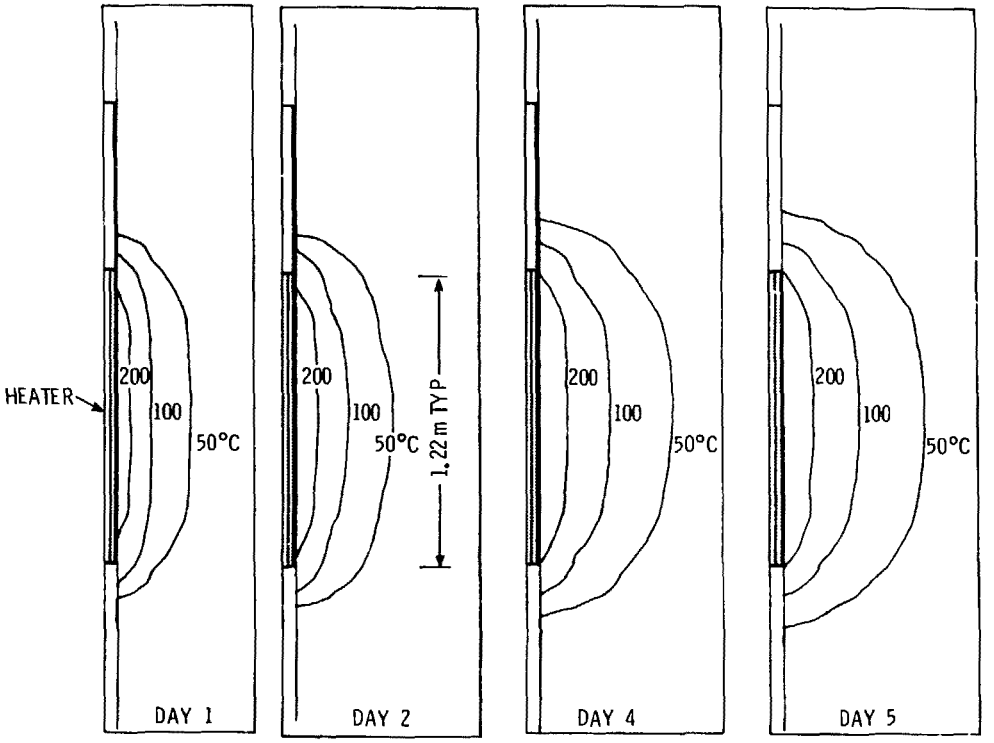

FIGURE 9. CALCULATED ISOTHERMS AT FOUR TIMES FOR MODEL HEATER; 2.0 kW INPUT POWER.

Figure 10 compares the time scaled temperature histories for a 5 day model and a 61.25 day full scale (prototype) test for 1.4 kW and 3.5 kW power input, respectively. Curves are given for eight non-dimensional radii. As previously mentioned, the surface temperature for the model is higher than for the prototype due to the greater L/D of model compared to the prototype (see Table II and Figure 2). At the end of the scaled time, the predicted rock surface temperature (R/R_o = 1) of the model is about 20°C higher than that of the prototype. This difference is very close to that predicted from Figure 2 (about 12%). This percentage difference in temperature is essentially constant at late times for R/R_o out to about 10. Note that the temperatures are very similar near the start of the test, before the influence of the different lengths can be felt. Based on this comparison (maximum predicted differences about 12%), it is felt that the 1.4 kW model test is a reasonable thermal evaluation of the argillite thermal response.

Figure 11 compares expected temperatures for the 2.0 kW scale test with the 3.5 kW prototype. In this case, the scale test temperatures are sufficiently above the prototype test so that a significant overtest occurs.

STRUCTURAL PREDICTIONS

Thermomechanical stresses are developed in the argillaceous rock mass surrounding a heater because of non-uniform temperature distributions radially outward from the heater. One of the purposes of the small scale heater tests was to determine, prior to committing the large heater, if the thermal stresses were great enough to cause gross failure of the bore hole in which the heater was placed. Although there was no instrumentation in the scaled heater experiments for measuring stresses or displacements, some crumbling/spallation of the rock was observed in the bore hole just above the heater in the 2.0 kW overtest condition.

The stress calculations for the scaled heater tests were performed using the two-dimensional finite element code, SASL.[5] The transient temperature

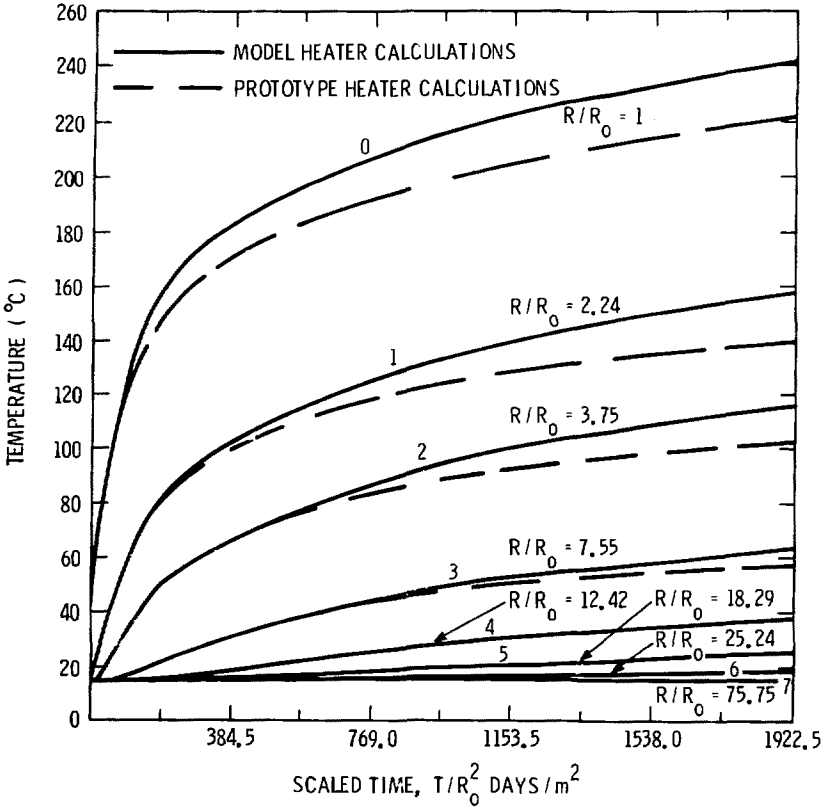

FIGURE 10. COMPARISON OF COMPUTED TEMPERATURES AS A FUNCTION OF SCALED TIME FOR MODEL (1.4 kW) AND PROTOTYPE (3.5 kW) HEATERS AT SEVERAL STATIONS RADIALLY OUTWARD FROM L/2 STATION OF HEATER.

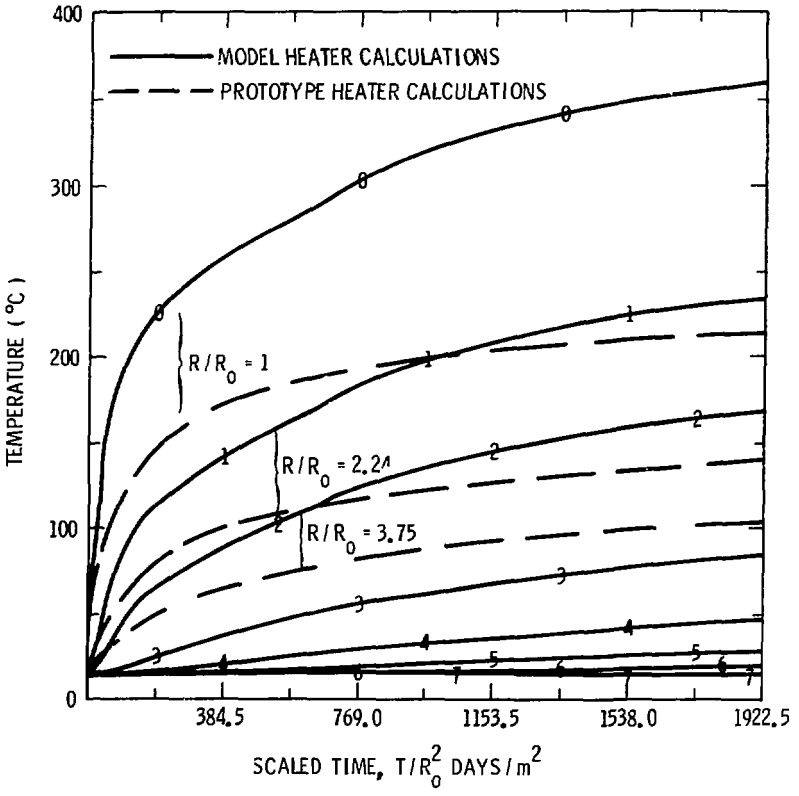

FIGURE 11. COMPARISON OF COMPUTED TEMPERATURES AS A FUNCTION OF SCALED TIME FOR MODEL (2.0 kW) AND PROTOTYPE (3.5 kW) HEATERS AT THREE STATIONS RADIALLY OUTWARD FROM L/2 STATION OF HEATER.

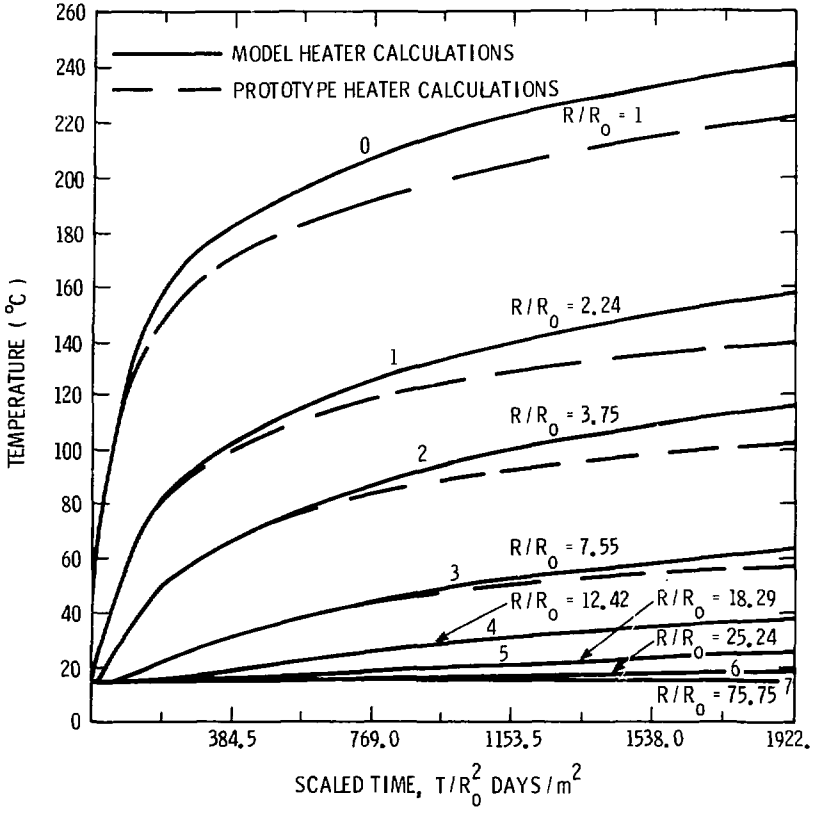

FIGURE 10. COMPARISON OF COMPUTED TEMPERATURES AS A FUNCTION OF SCALED TIME FOR MODEL (1.4 kW) AND PROTOTYPE (3.5 kW) HEATERS AT SEVERAL STATIONS RADIALLY OUTWARD FROM L/2 STATION OF HEATER.

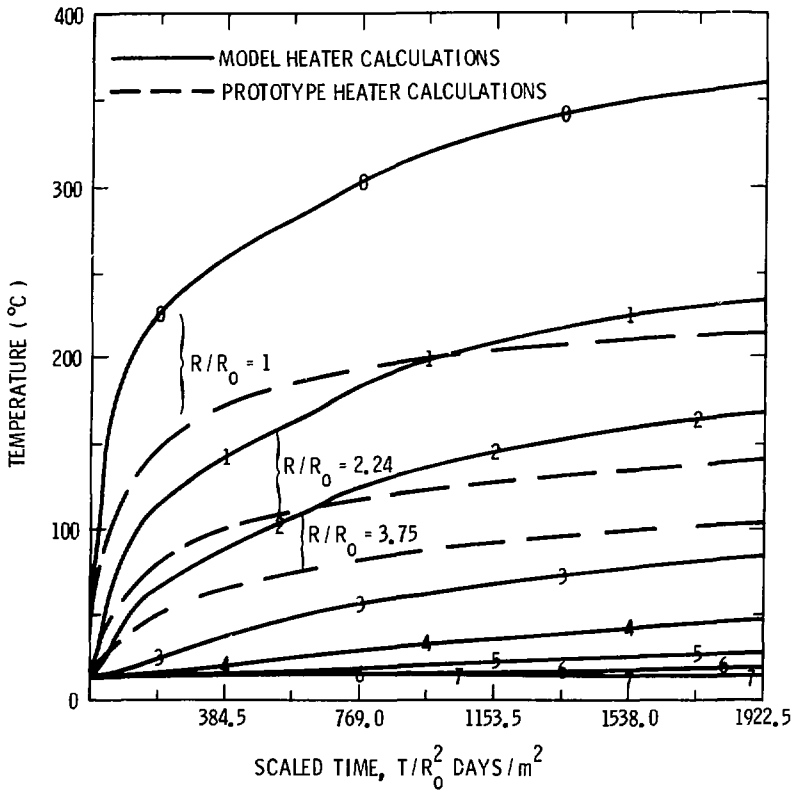

FIGURE 11. COMPARISON OF COMPUTED TEMPERATURES AS A FUNCTION OF SCALED TIME FOR MODEL (2.0 kW) AND PROTOTYPE (3.5 kW) HEATERS AT THREE STATIONS RADIALLY OUTWARD FROM L/2 STATION OF HEATER.

distributions, obtained from the thermal analysis, were written onto a permanent file and then recalled by a stress code preprocessor. Due to the proximity of the heater to the surface of the earth, i.e., emplacement at a depth of only 22.6 m, pre-existing in situ stresses were not considered.

The finite element model used for these stress calculations is shown in Figure 12. It consists of 1260 four-node quadrilateral elements and 1342 node points. The overall geometry of the analysis region is identical to that described in the thermal prediction section. However, the thermal code, COYOTE, uses a different mesh generator than the stress code, CASL. This incompatibility is corrected by a preprocessor code which interpolates nodal point temperatures from the thermal finite element mesh to obtain values for the stress finite element mesh. The overall dimensions of the model extend only beyond where the effects of the heater are observed for the times of interest. At these boundaries, the normal displacements are assumed to be zero, whereas the top surface is stress free.

For these calculations, the mechanical behavior of the argillite was modeled as an isotropic, homogeneous thermoelastic solid. Measurement of the mechanical properties of argillite is continuing, with particular emphasis on the dependence of properties on moisture content and confining pressure. Only limited data are presently available concerning these effects.

The room temperature properties assumed for argillite are

$$E = 6900 \text{ MPa}$$

$$\nu = 0.14$$

$$\alpha_T = 13 \times 10^{-6} \, {}^{\circ}C^{-1} \quad .$$

Measurements to determine the temperature dependence of the base properties, and incorporation of these effects into the stress calculations, are discussed in detail in Appendix B. The resulting thermal expansion as a function of temperature is shown in Figure 13, and the pressure dependent failure surface is shown in Figure 14. All calculated stresses are reported as a margin of safety (FAIL R) defined in Figure 14 as the ratio A/B, where A is the calculated

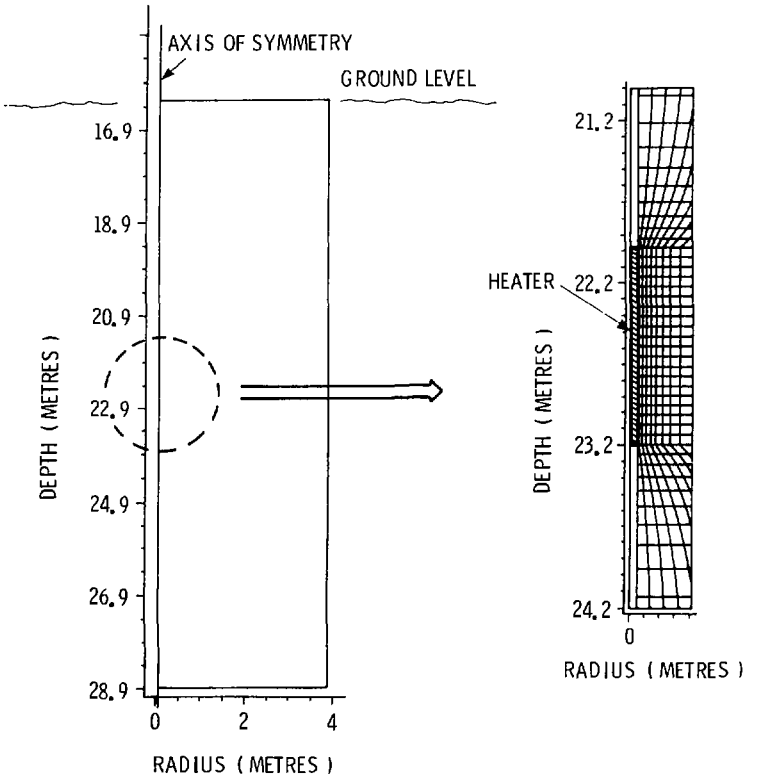

FIGURE 12. TWO-DIMENSIONAL AXISYMMETRIC FINITE ELEMENT MODEL OF NEAR SURFACE HEATER EXPERIMENT FOR STRESS CALCULATIONS.

distributions, obtained from the thermal analysis, were written onto a permanent file and then recalled by a stress code preprocessor. Due to the proximity of the heater to the surface of the earth, i.e., emplacement at a depth of only 22.6 m, pre-existing in situ stresses were not considered.

The finite element model used for these stress calculations is shown in Figure 12. It consists of 1260 four-node quadrilateral elements and 1342 node points. The overall geometry of the analysis region is identical to that described in the thermal prediction section. However, the thermal code, COYOTE, uses a different mesh generator than the stress code, CASL. This incompatibility is corrected by a preprocessor code which interpolates nodal point temperatures from the thermal finite element mesh to obtain values for the stress finite element mesh. The overall dimensions of the model extend only beyond where the effects of the heater are observed for the times of interest. At these boundaries, the normal displacements are assumed to be zero, whereas the top surface is stress free.

For these calculations, the mechanical behavior of the argillite was modeled as an isotropic, homogeneous thermoelastic solid. Measurement of the mechanical properties of argillite is continuing, with particular emphasis on the dependence of properties on moisture content and confining pressure. Only limited data are presently available concerning these effects.

The room temperature properties assumed for argillite are

$$E = 6900 \text{ MPa}$$

$$\nu = 0.14$$

$$\alpha_T = 13 \times 10^{-6} \, {}^{o}C^{-1} \quad .$$

Measurements to determine the temperature dependence of the base properties, and incorporation of these effects into the stress calculations, are discussed in detail in Appendix B. The resulting thermal expansion as a function of temperature is shown in Figure 13, and the pressure dependent failure surface is shown in Figure 14. All calculated stresses are reported as a margin of safety (FAIL R) defined in Figure 14 as the ratio A/B, where A is the calculated

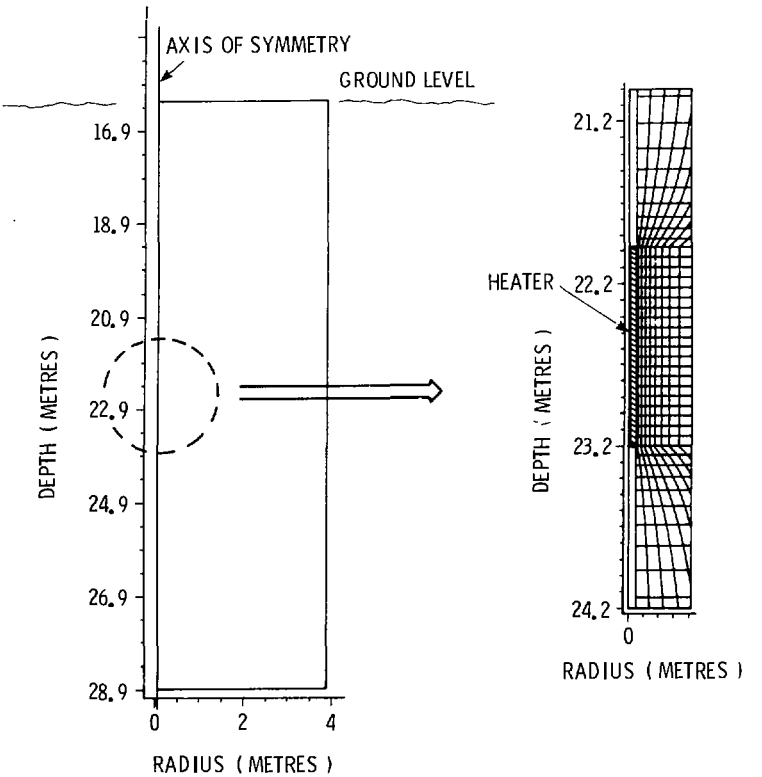

FIGURE 12. TWO-DIMENSIONAL AXISYMMETRIC FINITE ELEMENT MODEL OF NEAR SURFACE HEATER EXPERIMENT FOR STRESS CALCULATIONS.

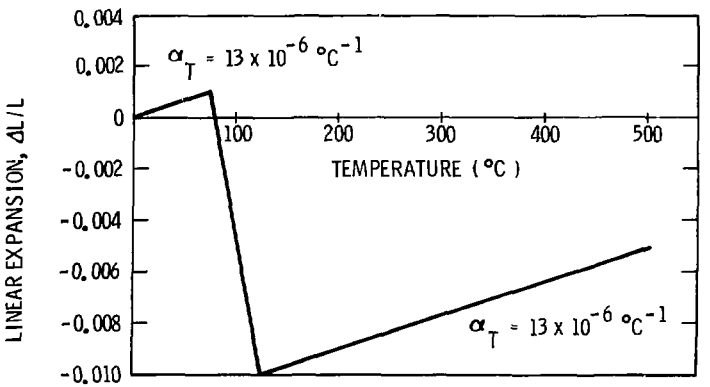

FIGURE 13. TEMPERATURE DEPENDENT THERMAL EXPANSION OF ARGILLITE INCORPORATING THE EFFECT OF DEHYDRATION SHRINKAGE.

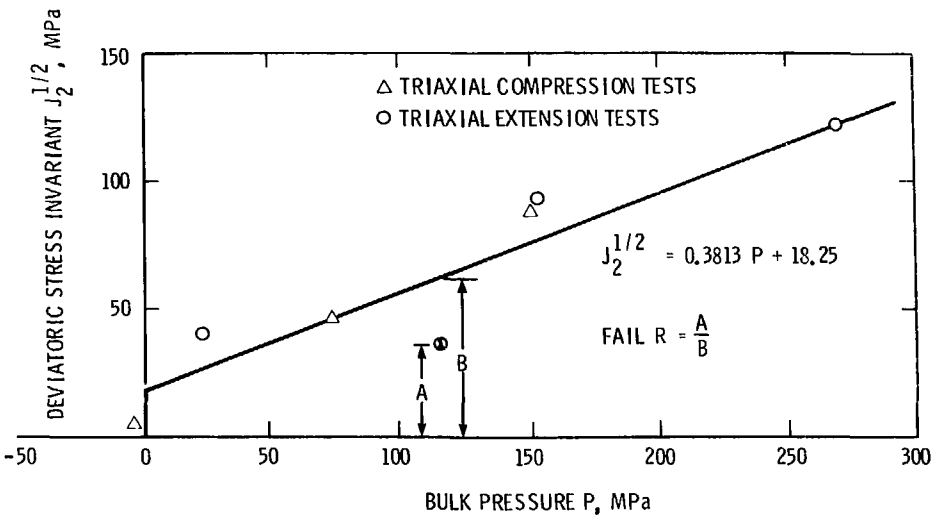

FIGURE 14. MOHR-COULOMB FAILURE SURFACE FOR ARGILLITE TAKEN FROM REFERENCE 8.

deviatoric stress at a given confining pressure and B is the calculated failure stress at the same pressure. Values of FAIL R greater than unity indicate predicted failure.

STRUCTURAL MODELING RESULTS

Stress calculations were performed for both the 1.4 kW and 2.0 kW heater power outputs and for times of 0.5, 1.0, 2.0, 4.0 and 5.0 days. The results are shown in the contour plots of FAIL R in Figures 15, 16 and 17. In Figure 15, contours of the failure parameter for a heater power output of 2.0 kW and a time of 5.0 days reveal the influence of the heater to be highly localized, extending less than one metre radially. It is, therefore, apparent that the radial and axial boundaries of the model are sufficiently removed from the heater so as to represent an infinite continuum.

Close up contours of the failure parameter are shown in Figures 16 and 17 for the two heater power outputs. The character of the material response is the same for the two power outputs, but the stress distributions are slightly different. At early times, in both cases, a region of the argillite directly adjacent to the heater is predicted to go into hydrostatic tension. This is a direct consequence of the effect of dehydration shrinkage above 75°C built into the thermal expansion coefficient. The peak magnitude of the calculated tensional bulk pressure is -52 MPa, a value which, in this constrained region, is fixed by the elastic modulus and expansion coefficient. Since no crumbling of the argillite was observed in this region of the bore hole, in either test, it is apparent that either: (1) the Eleana argillite can sustain a finite tensile stress in situ, or (2) that the contraction behavior was accommodated in situ by opening existing joints, or (3) that material was free to move into the contracting region, i.e., that the assignment of zero displacement boundaries is not valid.

The regions of hydrostatic tension adjacent to the heater were calculated to persist for the duration of the tests. However, by θ = 5.0 days, regions

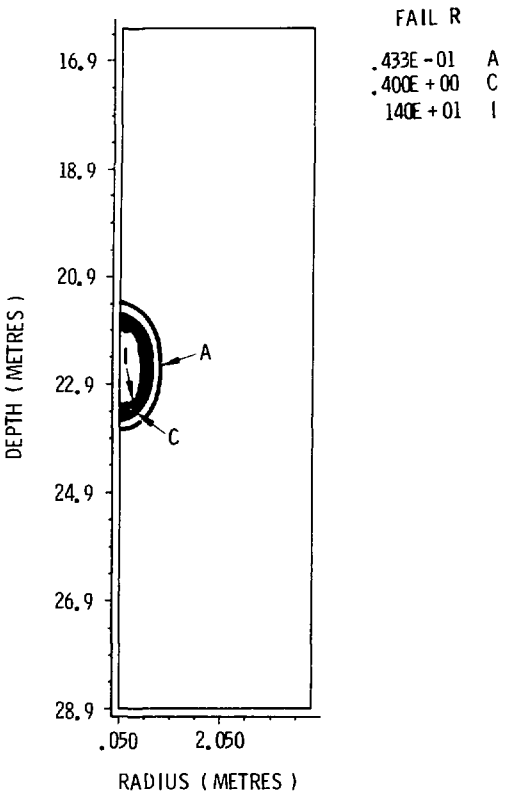

FIGURE 15. CONTOURS OF ROCK FAILURE PARAMETER FOR Q = 2.0 kW AND θ = 5 DAYS.

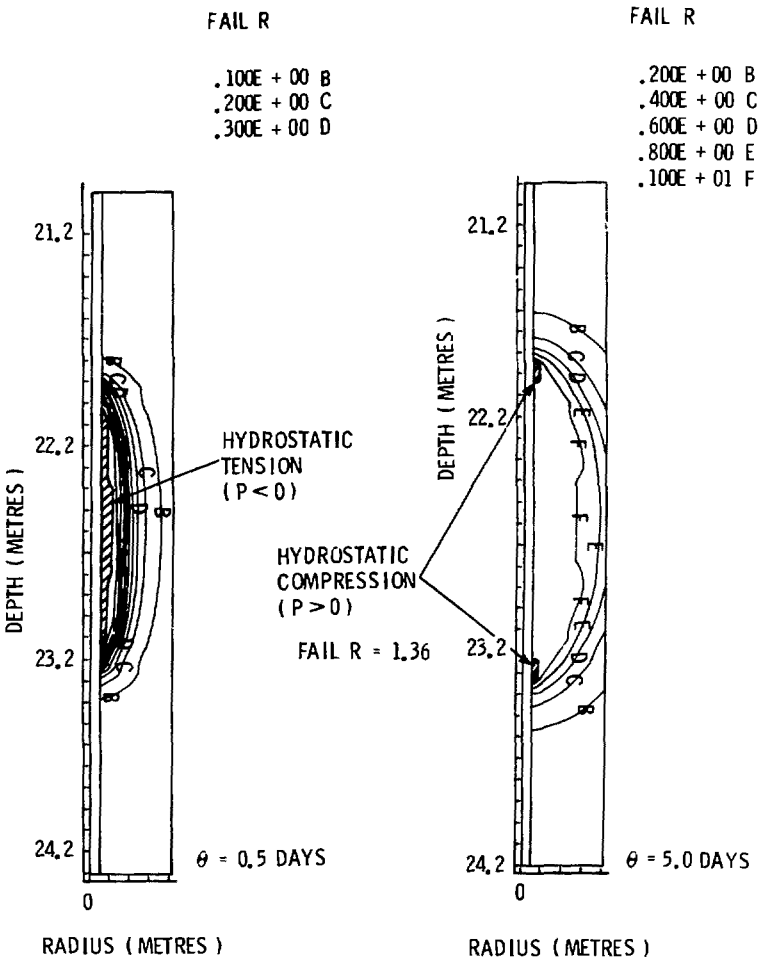

FIGURE 16. CONTOURS OF ROCK FAILURE PARAMETER FOR Q = 1.4 kW, AND θ = 0.5, 5.0 DAYS.

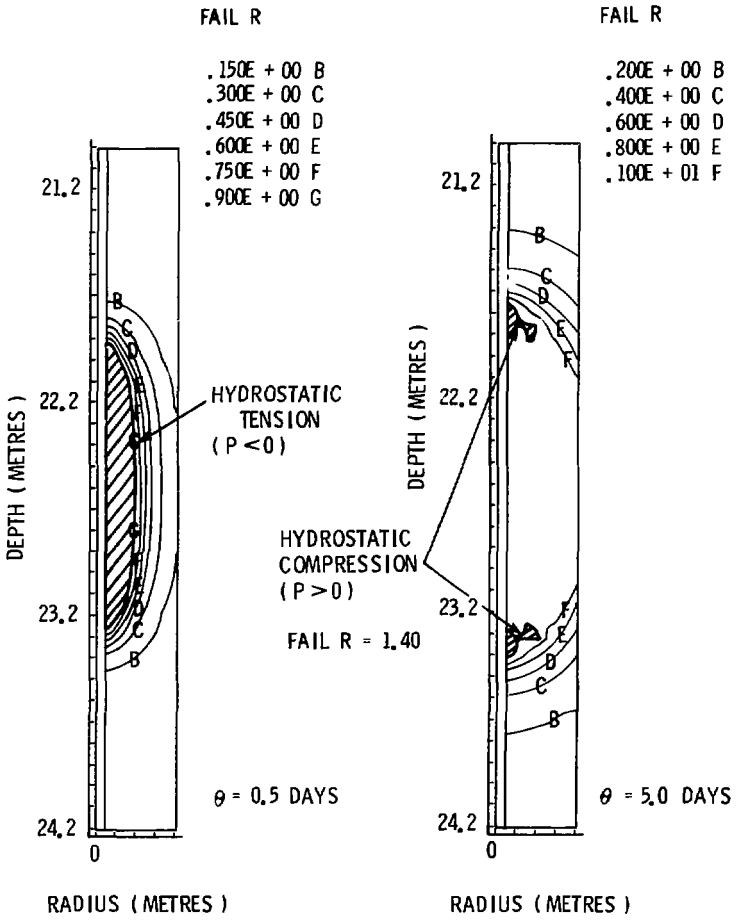

FIGURE 17. CONTOURS OF ROCK FAILURE PARAMETER FOR Q = 2.0 kW, AND θ = 0.5, 5.0 DAYS.

above and below the heater are predicted to be in a state of hydrostatic compression with a large deviatoric stress in both tests due to thermal mismatch between hot and cold zones. These zones, which are predicted to have failed, occur at earlier times in the 2.0 kW test than in the 1.4 kW test, and are somewhat larger. Pre and post test examination of the bore holes in which the tests were operated indicated limited degradation of the emplacement hole wall above the heater in the case of the 2.0 kW test, but none in the case of the 1.4 kW experiment. Experimental results and configurations are described in detail in the following sections.

EXPERIMENTAL DESCRIPTION

The scaled heater experiments described here were operated at power levels of 1.4 kW (Test 1) and 2.0 kW (Test 2). Power levels were held approximately constant using a Variac rheostatic controller. The test holes, nominally 0.10 m in diameter, were cased to 18.3 m with a nominal total depth of 24 m. The heater was suspended in the test hole by means of its power leads. Test 1 was initially operated on the bottom of its test hole for a period of approximately 2 hours. Due to a small amount of water pre-existing in the bottom of the hole, which was sufficient to cover the thermocouples at the heater centerplane after emplacement of the heater, maximum heater skin temperatures during this time did not exceed 94^{o}C, the boiling point of water at the elevation at which the experiments were conducted. After two hours, the heater was raised 1.1 m, such that the heater centerline (L/2) was at a depth of 22.6 m. The 2 kW scale experiment was operated in a different hole, with the heater centerline at 22.6 m throughout the test.

The cylindrical stainless steel (SS-304) heater used in these tests is 0.089 m in diameter with a 1.22 m heated length; it contains a single "Chromalox" wound-nichrome heater element bent into the shape of a "U" with a radius of curvature of approximately 0.03 m. The heater does not have an actively cooled junction section. Measurements taken as a function of time during the experiment include heater power, element temperature at heater centerplane, and two

"heater skin temperature" measurements at the centerplane. The thermocouples for these latter two measurements were Chromel-Constantan Type-E thermocouples, and were strapped to the outer heater surface. One thermocouple was strapped onto the skin directly opposite one leg of the heater element inside, and one halfway between the legs of the element, i.e., as far away from the element as possible. Thermal data were recorded on a strip printer at time intervals ranging from 1 minute to 1 hour, depending upon the stage of the experiment.

EXPERIMENTAL RESULTS

Temperature Data

Figure 18 gives the heater skin temperatures as a function of time for the 1.4 kW test, and compares these data with predicted temperatures. In this figure, the filled circles are for the centerplane skin thermocouple "between" the elements, and the open circles are for the thermocouple "adjacent" to the heating element. Thus, on the heater surface at the centerplane, there was up to 30°C, or ~10%, circumferential asymmetry in heater temperature. As is shown by comparing predicted and measured heater temperatures, experimental results agreed well with predictions. The deviation between average heater temperature and predicted heater temperature was 35°C (~3.5% of calculated heater temperature) at the end of the test (96 hours). At elapsed times of <2.5 hours, predicted temperatures were bracketed by those measured. A small deviation of measured and calculated results was noted after 2.5 hours into the experiment. The reasons for this deviation are not very clear, but may well relate to unmodeled variations in heater emissivity and rock thermal conductivity, to convection within the open hole above and below the heater, or to cooling effects of water and water vapor movement in the heater hole. No results of the 1.4 kW Eleana scaled heater experiment deviate significantly from predicted results or indicate the action of any major short-term or intermittent phenomena that are not included in the model.

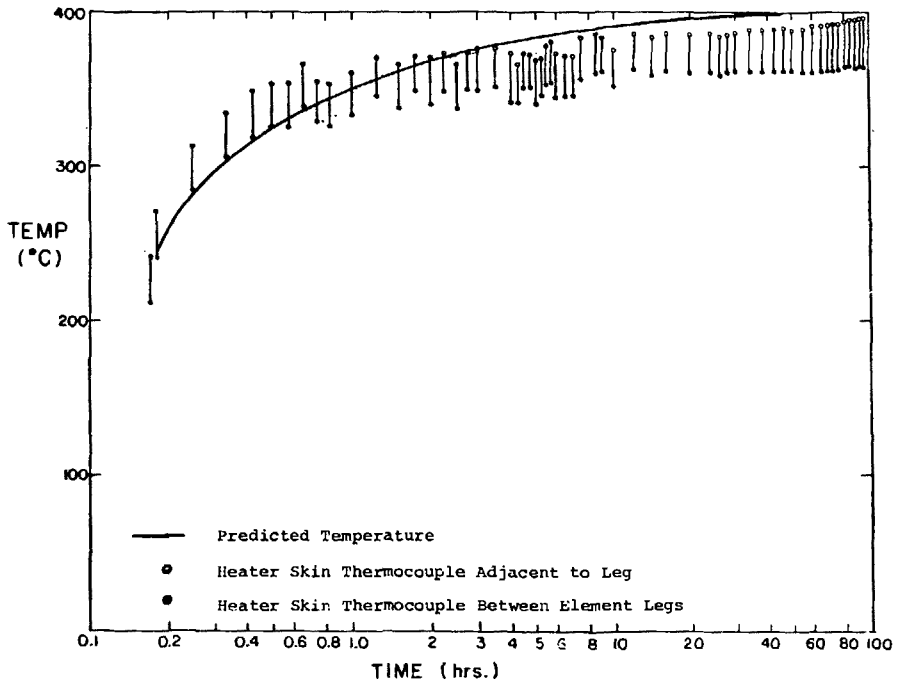

FIGURE 18. Measured Heater Surface Temperature Compared to Computed Temperature, 1.4 kW Test

Figures 19 and 20 give heater skin temperatures as a function of time for the 2 kW scaled heater experiment. As shown in Figure 19, predicted heater temperatures were bracketed by measured skin temperatures only for the first hour of the experiment. After this time, in addition to a general drift of heater temperatures below calculated values, three major "quenching" episodes occurred, during which temperatures of the thermocouple adjacent to the heater element (indicated by open circles in Figure 19) were quenched to 100°C or less. An expanded record of one of these excursions, that occurring between 17 and 25 hours elapsed time, is shown in Figure 20.

Data shown in Figure 20 indicate that TC-1, adjacent to the heater element, was repeatedly quenched to near 100°C, or below, for short periods of time. These decreases were consistently mirrored, but only slightly, by the element and TC-2 temperatures. There is little correlation of thermal output with the periodic decreases in TC-1 temperature. The temperature range to which TC-1 was repeatedly quenched, and the limited effects of this quenching on TC-2 and element temperature suggests that water was quenching TC-1, almost independently of the body of the heater. This may have been possible because the thermocouple sheaths were strapped onto the heater, and the TC-1 junction region was not fastened solidly to the surface.

Water Production

The initial 0.15 m water level in test hole 2 (TH-2), used for test 1, was sufficient to cover the centerplane thermocouples with the heater on the bottom of the hole. After operation of the experiment for a total of 96 hours and a cooling time of approximately 24 hours, the water level in TH-2 stood at 0.76 m. The water generation over the experimental time span is approximately 5.0×10^{-3} m^3 or $\sim 4 \times 10^{-5}$ m^3/hr.

Hole TH-3, used in test 2, was swabbed dry 18 hours before the initiation of the test, as were TH-2 and a nearby hole TH-1. After operation and cooling of the heater, over a total elapsed time of 171.5 hours, TH-3 contained 1.10 m of water, and TH-1 and TH-2 0.1 m. Using 0.10 m as the baseline production

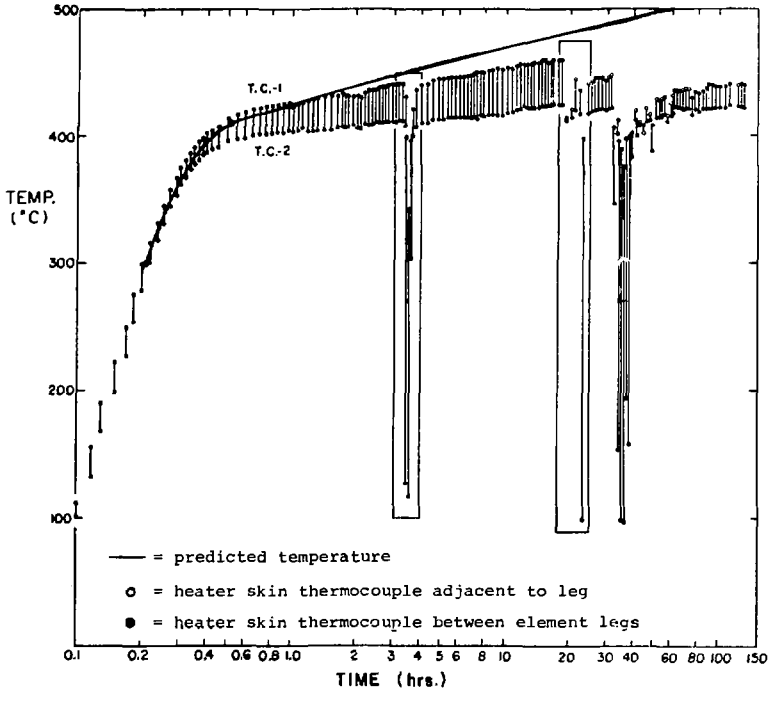

FIGURE 19. Measured Heater Surface Temperature Compared to Computed Temperature; 2.0 kW Test.

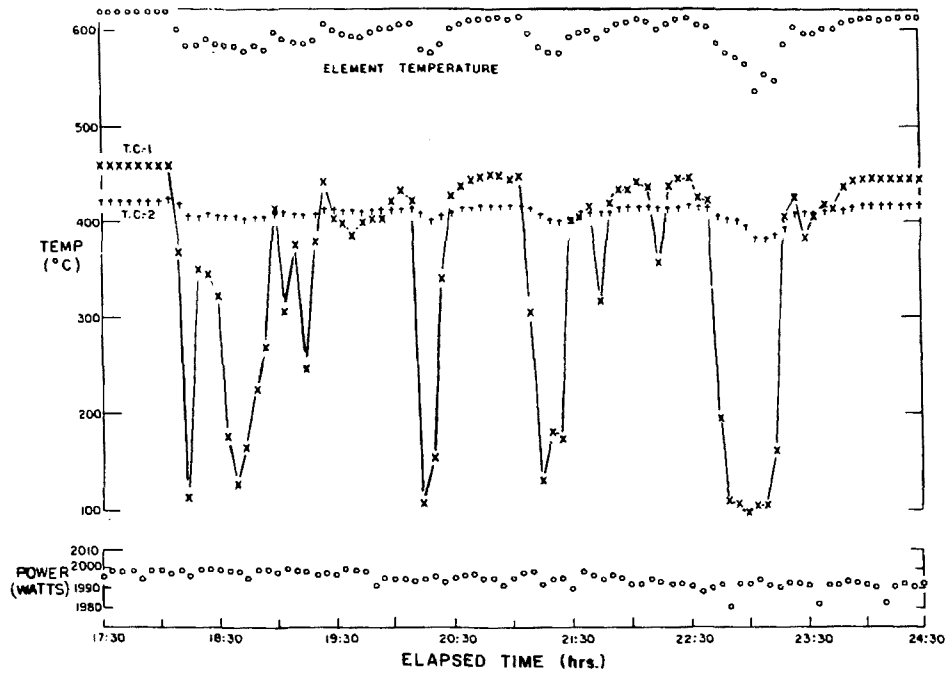

FIGURE 20. Measured Temperatures and Heater Power Between 17:30 and 24:30 Hours Elapsed Time; 2 kW Scaled Test.

(8×10^{-4} m^3), a total water generation of 8.04×10^{-3} m^3 or 4.7×10^{-5} m^3/hr during operation of test 2 is calculated.

Water generation during test 2 was, however, partially intermittent, as suggested by the periodic damping of TC-1 during this test. Termination of the heater after completion of the 2.0 kW scaled test shed light on both the method of water generation and thermocouple damping. As shown in Figures 21 and 22, a diagonal patch of deposit of material was noted on the heater skin after the test. This deposit is most likely related to a joint in the argillite. This area begins at the righthand margin of the field of view in Figure 22, and continues around to and slightly beyond the thermocouple sheath of TC-1. In addition, there are intermittent deposits between the TC-1 sheath and the heater casing, extending all the way down to the thermocouple bead, just within the field of view in Figure 22. Note that there is only slight alteration adjacent to the TC-2 sheath. Preliminary x-ray examination of the mineral deposits on the heater skin indicates that they consist of quartz, dolomitic calcite, kaolinite, and microcline. These observations are consistent with the interpretation that water gained access to TH-3 along a discrete joint and periodically ran along the groove between the TC-1 sheath and the heater skin as far as the thermocouple bead. Because the thermocouples were strapped onto the external heater surface, this mechanism allowed periodic quenching of TC-1, without major effects on either the heater element temperature or TC-2.

Bore Hole Examination

The calculated depth of radial penetration of the 100°C isotherm in the 1.4 kW test is 0.25 m (Figure 6). Approximating the volume inside the 100°C isotherm by a right circular annulus 1.22 m high with an outer radius of 0.25 m and an inner radius of 0.05 m, the total volume of rock that underwent boiling is predicted to be 0.23 m^3. Assuming that there is 7% porosity within the argillite, that the rock is fully saturated, and that all water within the volume above 100°C entered the heater hole, approximately 0.02 m^3 of liquid water should have been produced during test 1. The water level in the heater hole at the end of

FIGURE 21. Post-Test Photograph of Heater Used in Heater Test 2 Showing Surface Deposit Due to Water.

FIGURE 22. Post-Test Photograph of Heater Used in Heater Test 2 Showing Surface Deposit Due to Water.

the test should have then stood at a level of 2.15 m, as opposed to the observed 0.8 m. Assuming 70% saturation, as measured in near surface samples, the predicted water level is 1.5 m. Thus, while there may have been some near surface water that entered the heater hole during this scaled test, it can be stated with some certainty that not all the water boiled out of the rock entered the hole. Similar differences between calculated and measured water production also hold true for test 2.

Post test examination of TH-2 by means of a bore hole viewing camera after operation of test 1 indicated no noticeable degradation of the heater hole due to operation of the test. Post test examination of TH-3 after operation of test 2 (2.0 kW) indicated negligible degradation of the heater hole opposite the heater centerplane. However, there was a distinct region of "flaking" or "chipping," approximately two feet in width, centered approximately one foot above the top of the heater. This region is compared with unaltered walls in Figures 23 and 24. The wall appeared to have had many thin flakes or chips removed, with their long axes paralleling the hole wall. The chipping increased the hole diameter to approximately six inches. There was no evidence of any penetrative radial fracturing. Examination below the heater was eliminated by the water present in the hole. The location of the area of hole degradation in test 2 relative to the heater is in qualitative agreement with stress calculations described above.

CONCLUSIONS

The model tests described in this report indicated that major thermomechanical failure of in situ argillite would not be anticipated during the full scale heater test, if this test was operated at a power level of 3.5 kW. Qualitative agreement between predicted and observed thermal and thermostructural response was obtained, with the agreement being better in the 1.4 kW scaled test than in the 2.0 kW test, due to periodic ingress of water in the latter.

FIGURE 23. Pre-Test Bore Hole Scan.

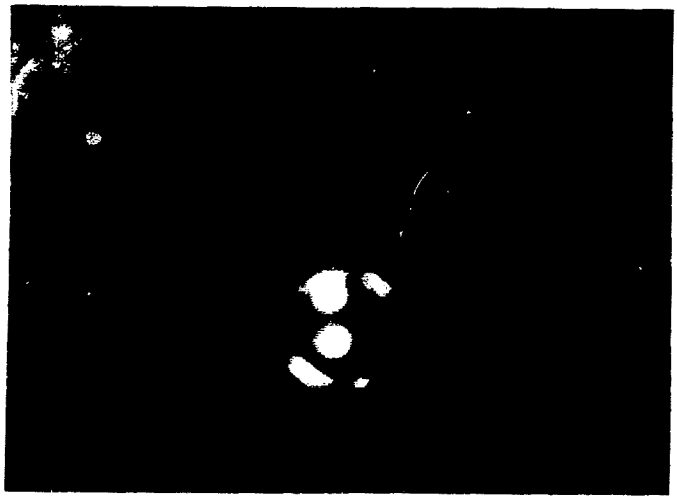

FIGURE 24. Post-Test Bore Hole Scan.

APPENDIX A

THERMAL PROPERTIES

Material thermal properties used in the analyses presented here and taken from Reference 2 are reproduced in Tables III and IV. All thermal conductivity tests were carried out at ambient pressure, which has two important implications for utilization of these data. First, significant dehydration of these samples almost certainly occurred even below 100°C due to evaporation. This dehydration is reflected in decreasing radial conductivities between 25°C and 100°C. Dehydration before boiling would not be expected to occur at depth. Secondly, the marked decrease in conductivities on boiling may well be partially invalid for experimentation at depth, since the conductivity decreases, shown in Table III, are due to the presence of air-filled microcracks and porosity. Bulk compressibility data on Eleana argillite indicate that existing microcracks are essentially closed at 1500 psi (10.3 MPa) confining pressure. Thus, a conductivity decrease of the magnitude reported in Tables III and IV would not be expected at depths where the confining pressure is greater than about 10.3 MPa.

In addition, it must be noted that due to sample size limitations and measurement technique constraints, conductivities in Table III are for measurements parallel and radial to the long axis of available core material, rather than parallel and perpendicular to bedding. In both samples, bedding was inclined at approximately 30° from perpendicular to the core axis. Thus, the radial conductivity measurements, made by means of a transient line source technique, reflect at least some heat transport across layering, and should be slightly low for transport parallel to layering. Likewise, the axial conductivity measurements, made by means of a guarded end plate technique, are probably slightly higher than for transport truly perpendicular to bedding. Bedding in much of the Eleana argillite is quite massive and difficult to see macroscopically; hence, the effects of measuring the conductivity at roughly 30° to the

material principle axes are not expected to be major. An axisymmetric thermal model necessarily ignores the presence of inclined layers; hence, the thermal conductivity data are consistent with the modeling.

The measured specific heats (Table IV) were modified by removing the singular spike occurring at 100°C and replacing it with the heat of vaporization of 3% by weight water added to the specific heat of the matrix. This was required because the technique used in collecting the data in Table IV does not account for possible water evaporation during sample preparation. While this handling of the heat capacity accounts for the heat absorbed by in situ water volitization, no effort was made to account for heat transfer due to convection of liquid or vapor within the rock. For compatibility with the internal workings of the computer code and with the thermal conductivity data, the vaporization of the pore water and loosely held montmorillite-bound water was assumed to occur over the temperature range of 55°C to 105°C.

APPENDIX B

MECHANICAL PROPERTIES

Ultrasonic measurements were made to provide a preliminary indication of the temperature dependence of the elastic modulus.[6] These tests were performed on material which was moisture free. The results showed a relatively small change in longitudinal modulus (approximately 9%/100°C) above the room temperature value.

Thermal expansion data for the argillite is of three types. First, small (~1" in length) samples initially measured immediately after preparation in water show 1% to 2% linear contraction when held at 110°C for 24 hours (Table B1). This contraction, consistent with the known mineralogy of the Eleana argillite (see Reference 2), is assumed to be due to contraction of the montmorillonite and vermiculite interlayers in "illite" within the argillite. Since the "illite" content of the Eleana appears to be quite variable, such contraction upon clay dehydration would be variable in situ, both as a function of total clay content and of relative solid and fluid confining pressures. Second, ambient pressure expansion data have been collected on both "natural state" and pre-dried specimens of argillite (Table B1), under conditions which allow at least partial sample dehydration below 100°C. In such tests on natural state specimens, the argillite generally shows limited expansion to about 50°C, followed by ~1% linear contraction, with maximum contraction occurring near 125°C. Above 125°C, samples continuously expand, with α_T between 10 and 15 x $10^{-6}(^{\circ}C^{-1})$, to 500°C. Third, two measurements of thermal expansion have been made under confining pressure to a temperature of 135°C. These tests, conducted at pressures of 3.45 and 20.7 MPa on 5.1 cm diameter core samples, showed no region of values of α_T = 15 and 17 x $10^{-6}(^{\circ}C^{-1})$, respectively. Under these confining pressures, significant sample dehydration did not occur.

For preliminary calculational purposes, the effect of dehydration shrinkage was combined with the thermal expansion measurements above 100°C under ambient pressure and those collected below boiling temperature under confining pressure, to obtain the composite curve shown in Figure 13. In reality, dehydration shrinkage behavior is a function of total clay content and species as well as both solid and fluid confining pressures. In the near surface environment, however, initial solid confining pressures are negligible and if previously stated assumptions about temperatures of dehydration are valid, the expansion behavior used in the analysis is reasonable.

The material strength used in the mechanical modeling were taken from data obtained on Eleana argillite from the "Yacht" hole (Uel1) on the Nevada Test Site.[8] These are triaxial compression and extension data in which the principal stress difference, $\sigma_1 - \sigma_3$, is reported as a function of the confining pressure, σ_3. The effect of the intermediate principal stress is not included since, under these test conditions $\sigma_2 = \sigma_3$. For this analysis, the failure strength was represented by a three-dimensional formulation, in terms of a stress deviator, $J_2^{\frac{1}{2}}$, and the bulk pressure, p, (compression was taken to be positive):

$$p = 1/3(\sigma_1 + \sigma_2 + \sigma_3) \quad ,$$

$$J_2^{\frac{1}{2}} = \sqrt{\frac{(\sigma_1 - \sigma_2)^2 + (\sigma_2 - \sigma_3)^2 + (\sigma_1 - \sigma_3)^2}{6}} \quad ,$$

where,

$\sigma_1, \sigma_2, \sigma_3$ = principal stresses.

The resulting test data are plotted in Figure 14. The failure strength was assumed to be the straight line bounding the lower scatterband. All calculated stresses are reported as a margin of safety (FAIL R) defined in Figure 14 as

the ratio A/B, where A is the calculated deviatoric stress at a given confining pressure and B is the calculated failure stress at the same pressure. Values of R greater than unity indicate predicted failure. All points with hydrostatic tension are assigned the R value of unity, i.e., the rock is assumed to have no tensile strength in situ. It is important to note that this Mohr-Coulomb failure surface is used in the analysis only to indicate locations in the geological media where the effective thermal stress has exceeded the strength. The material constitutive model remains thermoelastic, i.e., time independent. As the necessary mechanical properties data in argillite become available, non-linear, and time-dependent effects will be incorporated into future modeling.

TABLE B1

LINEAR THERMAL EXPANSION DATA, ELEANA ARGILLITE

A. Heating of sample Uel7e-993 segments for 24 hours @ 110°C

	$\delta\ell/\ell_o$ (%)
1. Perpendicular to layering (3 samples) ⊥	-1.9 ± 0.2
2. Parallel to layering (3 samples) ∥	-1.2 ± 0.2

B. Ambient pressure contraction/expansion of "natural state" sample during heating

Sample	% Shrinkage to Minimum Length	$\alpha_{125-500°C}$ ($\times 10^{-6}$ °C^{-1})
Uel7e993 (perp.)(2 samples)	1.68	+11.9
Uel7e2200 (perp.)(2 samples)	0.37	+14.9

C. Ambient pressure expansion of "air dried" samples during heating (no contraction was observed)

Sample	α_{avg} ($\times 10^{-6}$ °C^{-1})
Uel7e2200 ⊥ (3 samples)	13.1 (25°C-500°C)
Uel7e1400 ⊥ (2 samples)	11.2 (25°C-500°C)
Uel7g370 ⊥ (3 samples)	8.7 (25°C-450°C)
Uel7g370 ∥ (2 samples)	10.0 (25°C-500°C)

D. Confined expansion to 135°C

Sample	Confining Pressure	$\alpha_{25°C-135°C}$ ($\times 10^{-6}$ °C^{-1})
Uel7e2387	500 psi	15
Uel7e2387	3000 psi	17

REFERENCES

1. David K. Gartling, "COYOTE--A Finite Element Computer Program for Non-Linear Heat Conduction Problems," SAND77-1332, Sandia Laboratories, Albuquerque, NM, June 1978.

2. A. R. Lappin and J. F. Cuderman, "1978 Eleana Argillite-Nevada Test Site; National Waste Terminal Storage Program Progress Report, 10/1/76 - 9/30/77," Y/OWI-9, Office of Waste Isolation, p. 223-230, 1978.

3. Touloukian and Dewitt, Thermal Radiative Properties, Metallic Elements and Alloys, New York: IFI/Plenum Press, Figure 361A(1), 1972.

4. E. R. G. Eckert and W. O. Carlson, Int. J. Heat and Mass Trans., 2, p. 106, 1961.

5. Sandia Laboratories Memo, J. H. Biffle, 5521, to Distribution, dtd 3/22/74, subject: SASL Computer Revision and Implementation.

6. Sandia Laboratories Memo, I. J. Fritz, 5132, to K. W. Schuler, 5521, dtd 10/25/78, subject: Ultrasonic Measurements on Shale.

7. Sandia Laboratories Memo, A. R. Lappin, 4537, to R. K. Thomas and K. W. Schuler, 5521, dtd 10/23/78, subject: Thermal Expansion of Eleana Argillite.

8. E. R. Simonson, S. J. Green, S. W. Butters, L. A. Rogers, and A. H. Jones, "Stress-Strain and Failure Response of the 'Yacht' Site Shale," TERRA TEK Tech. Report TR72-26, 1972.